HEAT TREATMENT OPTIMIZATION ON THE WEAR BEHAVIOR OF A LOW STEEL NI-B-CNT ELECTROLESS COATING ALLOY

Alaa Mohammed Hussein Wais[1], Noor Aleslam Maher Shakir [1], Zainab Al-Khafaji[2,3,*], Shams Ahmed Salim[1], Hasanain Hayder Jawad[1], Zainab Mohammed Ahmed[1], Tabarek Salam Dakhil[1], Zainab Mohammed Mahdi[1]

[1]Biomedical Engineering Department, College of Engineering and Technology, Al-Mustaqbal University, 51001 Hillah, Babil, Iraq.

[2]Scientific Research Center, Al-Ayen University, Thi-Qar, Iraq

[3]Department of Civil Engineering, Faculty of Engineering and Built Environment, Universiti Kebangsaan Malaysia, 43600 UKM Bangi, Selangor, Malaysia. p123005@siswa.ukm.edu.my; https://orcid.org/0000-0002-5450-7312

[*]Correspondence: p123005@siswa.ukm.edu.my; Tel.: (+964 781 812 0132)

AJME 2025, 23 (3); https://doi.org/10.5281/zenodo.17218204

***ABSTRACT**: This work aimed to conduct a statistical analysis of the influence of heating treatment. Using the response surface methodology (RSM) technique, which is based on a core composite design, factors such as temp, deposition duration, and amount of CNTs on the wear behavior of electroless coatings (Ni-B-CNT and Ni-B) on low-alloy steels were investigated. The impacts of the heating treatment temp and deposition duration on the wear rate were evaluated for specimens heated to various CNT amounts (0, 35, and 0.7%). Specimen wear is accelerated by increasing the temperature and deposition duration between 350 and 400 degrees Celsius and then increasing the deposition temperature between 400 and 450 degrees Celsius. The wear rate of materials depends on several material and feature properties, including the topography, hardness, and frictional coefficient, in addition to the wear test conditions.*

***KEYWORDS**: Electroless coating; Microhardness; Heating treatment; RSM, rate of wear*

1 INTRODUCTION

Aqueous solution electroplating, which includes both electroplating and electroless plating, has recently gained widespread attention because of its many advantages, including ease of use, great deposition rates, affordability, uniform preparation of the coating layer (Dawood et al., 2020; Haleem et al., 2024; Jabor et al., n.d.; Radhi et al., 2024; RADHI et al., 2023), and promising end findings, such as high resistant to wear, hardness and anti-corrosion features (AL-ABBOODI et al., 2024; Al-Dulaimi et al., 2024; Boccaccini & Zhitomirsky, 2005; Jasim Ahmed Jasim; et al., 2024; Mohammed & Al-khafaji, 2023; Sattar et al., 2023). Compared with metal deposition in aqueous solutions, electroless nickel plating is a better-known method that has undergone significant changes since its discovery by Branner and Riddell in 1946. Unique features of the method include amorphous and/or microcrystalline deposits, significant reflectivity, low frictional coefficient and resistivity, reasonable wear, and abrasion resistance, uniformly great hardness and thickness, good solderability, and excellent corrosion resistance. Electroless coatings have applications in a variety of areas, including MEMS, EMI, heat exchangers, reactor membranes, powder metallurgy, and bacterial adhesion reduction. Compared with electrodeposition technology, electroless plating technology has the advantage of thickness uniformity (Barman et al., 2019; Bonin et al., 2020; Nabhan et al., 2023). In 1989, when the electroless Ni-B plating method became mature, repeatable, and scalable, it was adopted as a mass-production method. Much attention was given to the electroless Ni-B plating method to improve the surface quality of various substrates (Alaa Mohammed Hussein Wai et al. Alaa Mohammed Hussein Wai et al., 2019; Vitry et al., 2012). In many industries, electroless Ni-B plating technology is generally considered superior to Ni-P plating technology and more attractive (Vitry et al., 2022). Researchers have not performed much research on the vacuum Ni-B heating treatment (Bülbül et al., 2012). There is more emphasis on improving the mechanical features, resistance to wear and corrosion, and coating of nanocomposite materials. Other suitable solid

lubricants for use as nanocomposite coatings include Ni-P-CNT (Wang et al., 2016), CuCNT (Tsai et al., 2017), PTFE (Wan et al., 2016), and MoS2 (He et al., 2016). Utilizing statistical design methods involving RSM is attractive because fewer experimental runs are required to determine the relationship between deposition parameters and film properties. Furthermore, statistical design methods can display precise and valuable information about the meaning of the detected trends (Marciano et al., 2010).

This study aims to comprehensively examine the influence of crucial heating treatment parameters—deposition temperature, time, and carbon nanotube (CNT) amount—on the mechanical properties and microstructural characteristics of electroless Ni-B-CNT and Ni-B coatings on low-alloy steel. Through experimental and statistical analyses, including RSM depending on a central composite design, the study evaluates how these variables impact critical features involving friction coefficient, rate of wear, and microhardness. By identifying the optimal heating treatment conditions, the research seeks to enhance wear resistance and mechanical performance, ultimately optimizing substrate properties and coating durability for low-alloy steels under various conditions.

2 EXPERIMENTAL WORK

2.1 Statistical Experimental

The Response surface methodology (RSM) was used to determine the ideal deposition conditions (max hardness, reduced wear rate, and reduced frictional coefficient). Therefore, several parameters (e.g., the temp at which the CNTs are deposited, the duration of the deposition process, and the amount of the CNTs) influence the reaction to optimize it. The response surface methodology can estimate the impacts of parameters on an individual basis, as well as the response of parameters to each response variable, and define the relationships between responses and parameters (Bezerra et al., 2008). Using Design Expert v10.0, the work, analysis, and experimental design were reviewed in three programs) is used in statistical experiments. A CCD or central composite design. Twenty heating treatment experiments were conducted. Table 1 illustrates the control levels for the CNT amount, duration, and deposition temp. Table 2 illustrates the design point blends arrangement and the comparable experimental response magnitudes..

Table 1. Parameters and range of differences.

Factor	Variations Ranges
Duration (hr)	1-4
Amount of CNTs (%)	0-0.35-0.7
Temp. (oC)	350-400-450

Table 2. Comparable design blends and experimental responses for heating treatment.

No.	A: Duration (h)	B: CNT %	D: temp. (oC)	Hardness (HV)	Specific Wear rate (mm3/N m)*10-4	frictional coefficient
1	1.00	0.00	350	560	2.4	1.25
2	2.50	0.00	400	700	1.7	0.8
3	1.00	0.70	450	600	2.8	1.15
4	4.00	0.35	400	1100	0.04	0.5
5	2.50	0.35	400	1050	0.048	0.49
6	2.50	0.35	450	850	0.5	0.55
7	2.50	0.35	350	856	0.5	0.56
8	2.50	0.35	400	1050	0.0681	0.55
9	2.50	0.70	400	712	2	1.17
10	4.00	0.70	350	725	1.8	0.99
11	1.00	0.00	450	580	2.7	0.98

12	4.00	0.70	450	740	1.5	1.1
13	4.00	0.00	450	750	2	0.85
14	2.50	0.35	400	1054	0.05	0.51
15	2.50	0.35	400	1056	0.051	0.52
16	4.00	0.00	350	740	1.3	0.89
17	2.50	0.35	400	1050	0.04	0.49
18	2.50	0.35	400	985	0.26	0.581
19	1.00	0.70	350	640	2.8	1.2
20	1.00	0.35	400	832	1	0.56

Table 3. Chemical compositions of AISI 4340 steel.

Element	C	Si	S	Mn	P	Cr	Ni	Mo	Fe
Standard AISI	0.3-0.45	0.2-0.4	Max 0.04	0.5-0.8	Max 0.04	0.6-0.9	1.25-1.75	0.15-0.25	Bal.
W%	0.36	0.29	0.01	0.67	0.01	0.81	1.3	0.15	Bal.

2.2 Preparation of the substrate)

Steel type 4340 was the substrate metal used in this project. Samples with dimensions of (2 and 1 cm) diameter and height, respectively were utilized as the substrate. Table 3 illustrates the chemical analysis findings for 4340 steels.

Each specimen was ground and polished. The materials (30, 60, and 60 g/L) of NaOH, NaCO3, and NaPbO4, respectively were immersed in a solution at 70°C for one minute. The electrolyte was magnetically stirred with a power supply (5 volts), removing any oil from the metal surface. After the samples had dried, they were immersed in the coating solution.

2.3 CNT Ball-Milling

MWCNTs with diameters ranges of (20–30 and 5–10) nm for outer and inner diameter, re-spectively, and a purity of over 95% were purchased from US Research Nanomaterials, Inc. Figure 1 illustrates images of the as-received and ball-milled CNTs taken via field emission scanning electron microscopy at MIRA3 TESCAN in Iran. The image illustrates how ball-milled carbon nanotubes (CNTs) decrease in size and become more upright to improve CNT dispersion in an electroless bath. Carbon nanotubes must be evenly distributed in the metallic matrix phase of an electroless Ni-B coating to prevent agglomeration and ensure a homoge-neous and stable dispersion. SDS surfactants (so-dium dodecyl sulfate) should be used with CNTs and combined with water for 45 minutes via an ultrasonic device.

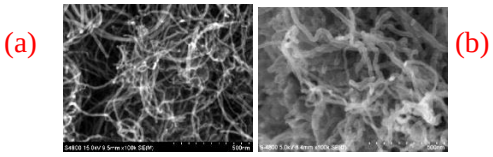

Fig. 1. FESEM images of (a) as-received CNTs and (b) ball-milled CNTs.

2.4 Preparation of the Electroless Bath

After the surface preparation, the electro-less plating bath was prepared at the amounts il-lustrated in Table 4. The Ni-B coating was applied to the substrate via a coating process. The pH of the coating bath was between 12 and 14. This process was carried out for one hour at 95 ± 1 °C for the electroless Ni-B coatings. A magnetic stirrer has been utilized to mix the bath solution during coating, reducing ion amount fluctuations. A monastery was used every ten minutes to create a uniform layer thickness. The Ni-B-CNT coating was applied at two different CNT amounts: 0.3 g/L and 0.7 g/L. Part II of the electroless deposition experiment is illustrated in Figure 2.

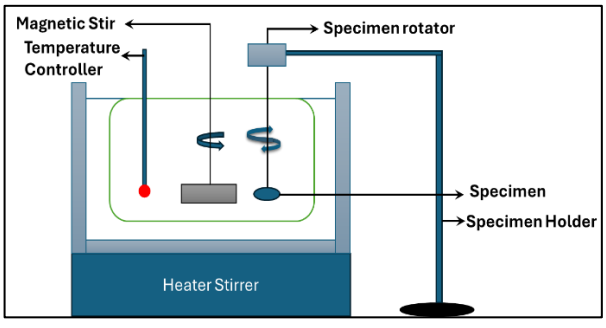

Fig. 2. Setup of the electroless deposition process experimentally.

Table 4. Operational conditions for the electroless bath.

Bath composition	Quantity
NiCl2.6H2O	24 g/l
NaBH4	0.8 g/l
Ethylenediamine 98%	60 ml/l
Lead Nitrate	0.02 g/l
NaOH	90 g/l
Sodium Dodecyl Sulfate	0.2 g/l
Carbon nanotube (CNT)	0, 0.35, 0.7 g/l
Operational conditions	
pH	13
Temp	95 oC
Duration of immersion	1 hour

2.5 Heating treatment of Coated Specimens

This work carried out the annealing process in a heating treatment vacuum furnace. The coated specimens were immersed at 350, 400, or 450 degrees Celsius for one, two, three, or four hours. They were then cooled to room temperature in an oven.

2.6 Characterization

The coating layers microhardness was determined using a load of 25 g for 15 seconds and a Vickers hardness tester. The average magnitude was then determined. The pin-on-disc method (ASTM G 99 standard) (Conshohocken, 2017) was utilized for the wear test. The load used was 10 N. The sliding distance was 376 m, and the sliding speed was 0.01 m/s. The disc was made of steel carbide. To determine the weight loss caused by the coating, the samples were weighed with a sensitive balance after and before the wear test, the formula for calculating the specific wear rate is.

Ws= w/(lL)

Whereas

L=the normal load.

W=the mass loss

L=the sliding distance.

3 FIDINGS AND DISCUSSION

3.1 Surface morphology

The coated specimen surface morphology is illustrated in Figure 3, with the smooth Ni-B specimen microstructure resembling a cauliflower, as illustrated in the image in Figure 3a. Lubricants maintained under adhesive wear conditions can benefit from this structure (Biswas et al., 2022; Mukhopadhyay et al., 2018). While a smaller portion of the CNTs protruded from the coated surface, the majority of the CNTs were fixed in the matrix by particle dispersion. In contrast, the CNTs were located on the sample surface with 0.35 g/L CNTs, as illustrated in Figure 3b. Moreover, a significant shift in microstructure was detected for the sample with 0.35 g/L CNTs. This observation makes sense and increases the uniformly coated surface area, with the low amount of CNTs allowing them to fill gaps and crevices. The size of the nodules increased when the CNT amount was increased to 0.7 g/L. This result was associated with a more significant amount of decreased nickel in the electroless bath, which might have contributed to minimized nucleation, as illustrated in Figure 3c. Large particles around the Ni-B-0.7 g/L CNT specimen caused the detected CNT aggregation due to their significant amount, causing the CNTs to aggregate on the base metal, which in turn caused large particles on the specimen surfaces to take on shapes associated with Ni nucleation during CNT agglomeration. Figure three-dimensional also includes an image of the specimen at a greater magnification to further illustrate the CNT distribution.

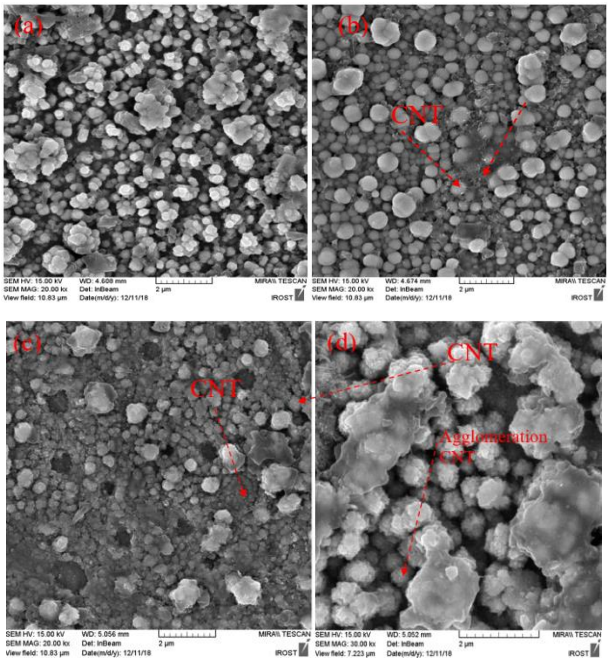

Fig. 3. FESEM images of the (a) Ni-B, (b) Ni-B-0.35 g/L CNT, (c) Ni-B-0.7 g/L CNT, and (d) Ni-B-0.7 g/L CNT specimens subjected to electroless coating.

3.2 Data analysis via RSM

Using Design Expert software, the relationships between the experimental factors (deposition temp,

CNT amount, and deposition) and the responses (hardness, wear rate, and frictional coefficient) were examined. Two essential steps in the modeling process are choosing an appropriate model to fit and demonstrating the model's efficiency (Ghafari et al., 2014). Using the F test and P magnitude, the significance of several models (two factors, linear, cubic, and quadratic) was determined. The findings revealed that a quadratic model adequately captured the relationships between the parameters and hardness, frictional coefficient, and rate of wear for specimens subjected to heating treatment (Tables 5-7).

.

Table 5. Wear rate fits for the heating treatment of the specimens.

Source	Sequential magnitude of P	Lack-of-fit Magnitude of P	Magnitude of F	
(Linear)	0.5151	< 1.00E-04	222.16	
(2F1)	0.9801	< 1.00E-04	301.31	
(Quadratic)	< 1.00E-04	0.0383	5.79	Propose
(Cubic)	0.5611	0.0091	17.04	Alias

Table 6. Frictional coefficient fits for heat-treated specimens.

Source	Sequential magnitude of P	Lack-of-fit Magnitude of P	Magnitude of F	
(Linear)	0.6529	< 1.00E-04	96.56	
(2F1)	0.9350	< 1.00E-04	128.63	
(Quadratic)	< 1.00E-04	0.0458	5.28	Propose
(Cubic)	0.0165	0.6255	0.27	Alias

Table 7. Hardness fits for heat-treated specimens.

Source	Sequential magnitude of P	Lack-of-fit Magnitude of P	Magnitude of F	
(Linear)	0.5757	1.00E-04	67.19	
(2F1)	0.9959	< 1.00E-04	91.95	
(Quadratic)	< 1.00E-04	0.0222	7.57	Propose
(Cubic)	0.8058	0.0030	28.90	Alias

An analysis of variance (ANOVA) is performed to examine the chosen model significance. Tables (8–10) present the findings of the ANOVA. The "last-of-fit" test is used to analyze the model's efficiency. The findings illustrate that for a quadratic model selected for the hardness, frictional coefficient, and wear rate for heating treatment of the specimen, the “misfit” is negligible. The quadratic model (F magnitude of 123.92) chosen for the wear rate is significant. The probability of noise leading to a model magnitude of F is only 0.01%.

Table 8. ANOVA findings for the wear rates of heat-treated specimens.

Source	Sequential magnitude of p	Magnitude of F	P-magnitude of prob >F	
(Quadratic)	Design	123.92	< 1.00E-04	significance
	Lack-of-fit	4.77	0.0522	insignificance
R2=98.64% Adj R2=97.84%				

Table 9. ANOVA findings for the frictional coefficient of the heat-treated specimens.

Source	Sequential magnitude of p	Magnitude of F	P-magnitude of prob >F	
(Quadratic)	Design	57.36	< 1.00E-04	significance
	Lack-of-fit	4.74	0.0518	nonsignificance
R2=96.36% Adj R2=94.86%				

Table 10. ANOVA findings for hardness for heat-treated specimens.

Source	Sequential magnitude of p	Magnitude of F	P-magnitude of prob >F	
(Quadratic)	Design	47.83	< 1.00E-04	significance
	Lack-of-fit	4.60	0.0538	nonsignificance
R2=94.46% Adj R2=92.49%				

Figure 5 depicts normal probability plots for the residuals of hardness, wear rate, and frictional coefficient associated with the heating treatment. The remaining values It is proposed that in a normal probability plot, the residuals exhibit a normal distribution as they closely resemble a straight line.

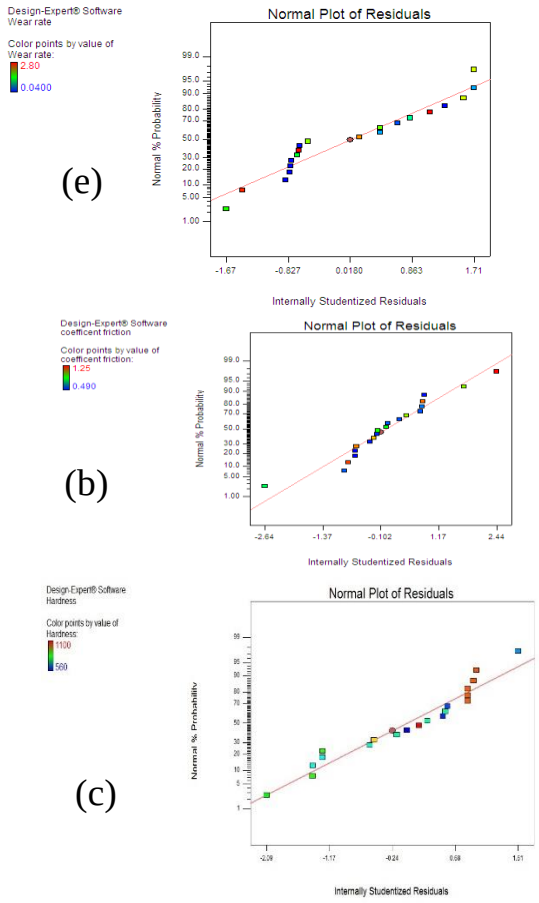

Fig. 5. Residual plots of the (a) rate of wear, (b) frictional coefficient, and (c) hardness of the as-annealed specimens.

Some terms (P higher than 0.05) were absent from the formulas because of the ANOVA findings. The ANOVA of the models illustrates that these terms are not significant. Terms that are not significant are removed backward. After eliminating the nonsignificant terms, the experimental data are subjected to "multiple regression analysis," and the resulting response formulas are given below.

1. The fitted wear rate model for the heating treatment of the specimen is explained in the following formula, the final equation in coded factors terms as follows:

Wear rate=+0.16+0.070*A-0.5*B+0.080*C-0.16*A*C+0.22*A2+0.24*B2+1.57* C2 (1)

Plots of the impacts of the deposition temp and duration on the wear rate during heating treatment of specimens with a constant CNT amount (0.35 g/L) are illustrated in Figures 6a and 6b. The figure illustrates how the specimen wear rate decreases with increasing deposition duration and temp from 350 to 400 degree centigrade and then increases with increasing temp from 400 to 450 degree centigrade. The wear rate of materials is determined not only by wear test parameters such as temp, atmosphere, lubricant type, perpendicular force, sliding speed, and pin type but also by a series of material properties and characteristics, including topography, hardness, elastic modulus, frictional coefficient and surface roughness (Shaikh et al., 2024).

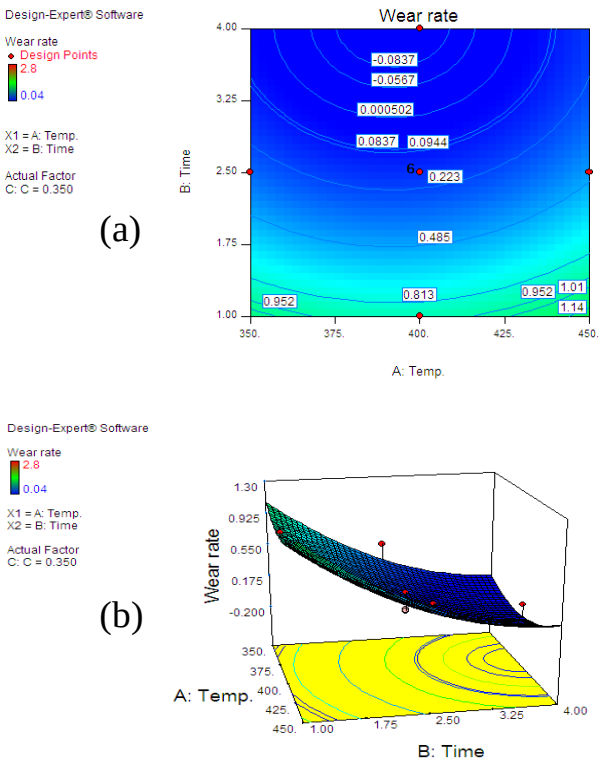

Fig. 6. Impacts of the deposition temp and duration on the wear rate during heating treatment of specimens with a constant amount of CNTs (0.35%): (a) 2D contour and (b) three-dimensional surface.

2.The fitted model of the frictional coefficient of heat-treated specimens is explained in the following formula, the final equation in coded factors terms as follows:

Friction of Coefficient =+0.5-0.026* A-0.081* B+0.084* C+0.049*A* B+0.046*A* C+0.51* C2 (2)

Figures 7a and 7 b illustrate plots of the impacts of the deposition temp and duration on the frictional coefficient for specimens heated to a constant amount of carbon nanotubes (0.35 g/L). As the temperature increases from 350 to 400 degree centigrade and from 400 to 450 degree centigrade, the frictional coefficient of the specimens decreases and increases, respectively.

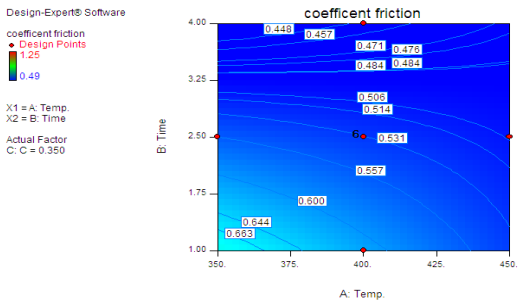

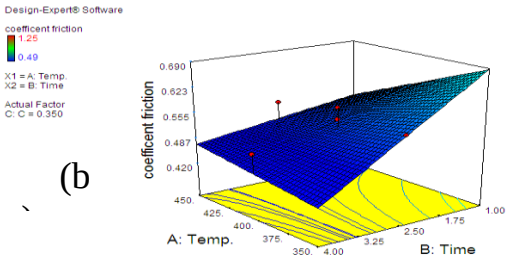

Fig. 7. Impacts of the deposition temp and duration on the frictional coefficient during heating treatment of specimens with a constant amount of CNTs (0.35 g/l): (a) 2D contour and (b) three-dimensional surface.

3. The hardness fitted model of the heat-treated specimens is explained in the following formula:

Hardness =+1009.12-0.100*A+84.30* B+8.70*C-104.13*A2-251.12*C2..... (3)

Figures 8a and 8 b illustrate plots of the impacts of the deposition temp and duration on the hardness of specimens subjected to heating treatment at a constant amount of carbon nanotubes (0.35 g/L). The figures illustrate how the hardness of the specimens increases by increasing deposition duration and temp from 350 to 400 degree centigrade; it decreases from 400 to 450 degree centigrade with an extra increase in the deposition temp and a reduction in the deposition duration.

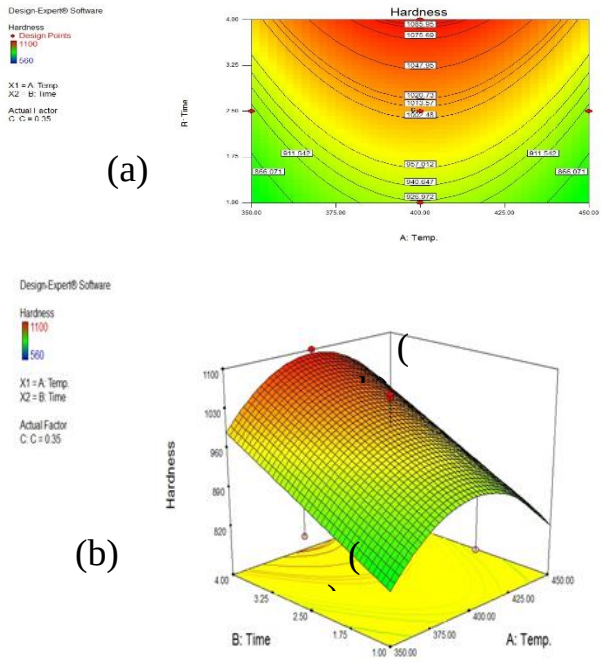

Fig. 8. Impacts of the deposition temp and duration on specimens' hardness pre-heating treatment at a constant CNT amount (0.35 g/l): (a) 2D contour and (b) three-dimensional surface.

4 THE OPTIMIZATION OF PARAMETERS AND RESPONSE

The Design Expert software is used for the findings optimization gained from the hardness, frictional coefficient, and rate of wear. For the heating treatment of coated electroless specimens:

The factor constraints and groups utilized during the optimization process are presented in Table (11). Table 12 illustrates the findings of RSM optimization for the reaction parameters (hardness, frictional coefficient, and rate of wear) and the contribution process parameters (deposition temp, duration, and amount of CNTs). As illustrated in Figure (12), the ideal design point (lower rate of wear, lower frictional coefficient, and maximum hardness) with a desirability magnitude of 0.9956 indicates the following: temp (397.03 °C), duration (4 hours), and CNT amount (0.35%)

Table 11. The factor constraints and groups utilized in optimizing the heating treatment of the coating electroless specimen.

Name	Goal	Lower Limitation	Upper Limitation
Temp.(oC)	Within range	350	450
Duration (hr)	Within range	1	4
CNT (%)	Within range	0	0.7
Hardness	Max	550	1100
Rate of Wear (mm3/Nm)	Min	0.04E-4	2.8 E-4
Friction of coefficient	Min	0.49	1.25

Table 12. Findings of RSM optimization parameters of the contribution process and response (hardness, frictional coefficient, rate of wear) for heating treatment of electroless specimens.

Number	Duration (hour)	CNT %	Temp. (0C)	Hardness (HV)	Specific wear rate (mm3/N m)*10-4	The frictional coefficient	(Desirability)
1	4	0.35	397.03	1092.9	-0.107062	0.447753	0.9956 Proposeed
2	4	0.39	398.41	1091.45	-0.0783494	0.463708	0.9950
3	4	0.32	391.21	1087.3	-0.105006	0.443409	0.9950

Figures (9-11) illustrate the optimal design point (a lower wear rate and frictional coefficient, and the greatest hardness).

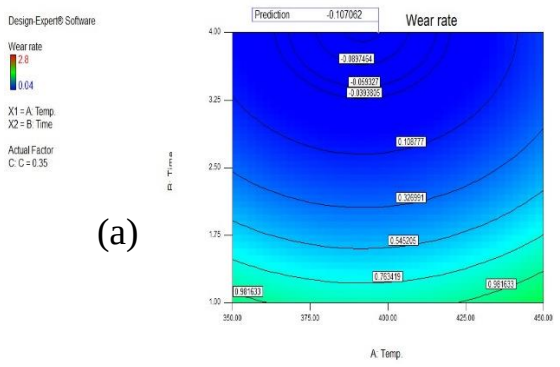

(a)

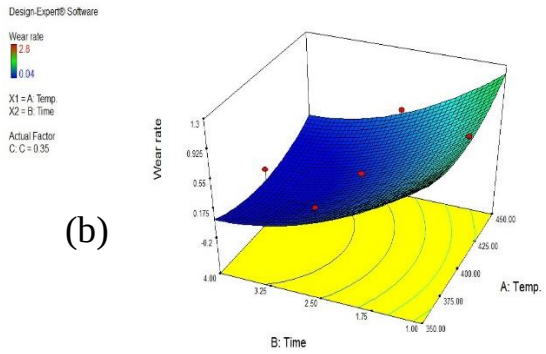

(b)

Fig. 9. A lower wear rate for heating treatment of electroloaded specimens: (a) 2D contour and (b) three-dimensional surface.

(

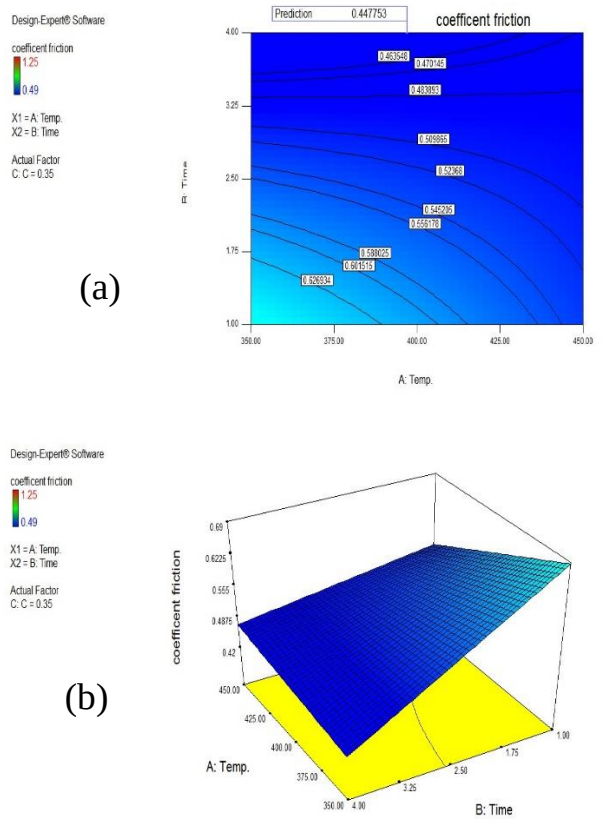

Fig. 10. A lower frictional coefficient for heating treatment of the electroloaded specimens: (a) 2D contour and (b) three-dimensional surface.

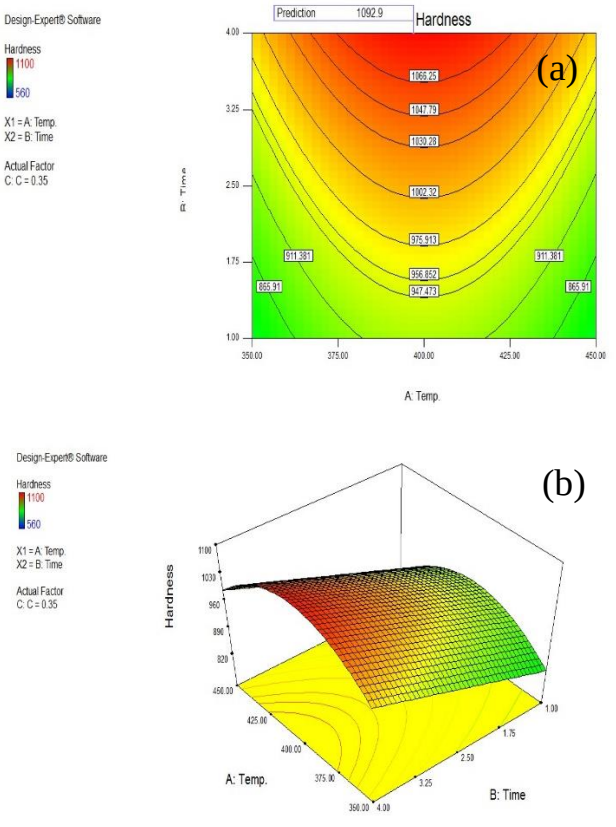

Fig. 11. The most incredible hardness for heating treatment of the electroloaded specimens: (a) 2D contour and (b) three-dimensional surface.

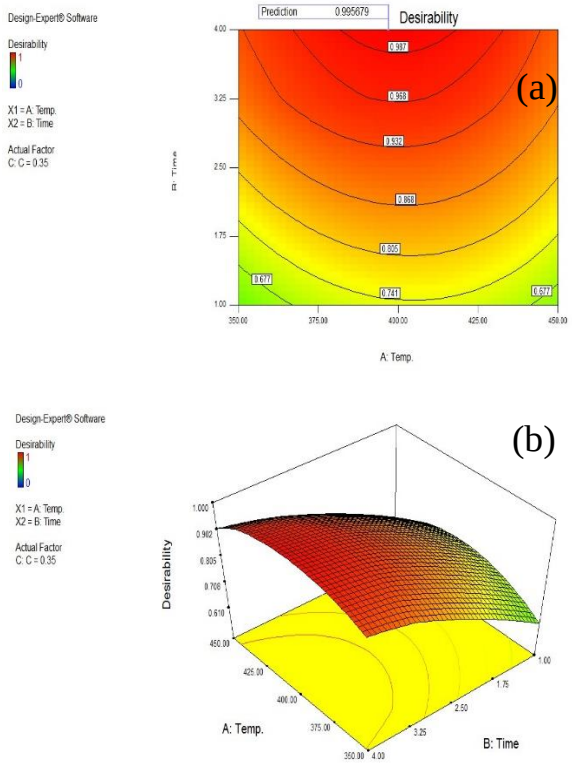

Fig. 12. Desirability contours of the lower wear rate, lower frictional coefficient, and most incredible hardness for the heating treatment of the electroplated specimens: (a) 2D contour and (b) three-dimensional surface.

5 CONCLUSIONS

In RSM was used to determine the impacts of heating treatment parameters (amount of CNTs, deposition temp and duration) on the hardness, wear rate, and frictional coefficient of the electroless coatings of Ni-B-CNT and Ni-B on AISI 4340 steel. The main conclusions are summarized here.

1. The extended model (Design Expert software) was used to calculate the regression coefficient (R-sq) for the electroless heating treatment of the coatings, and the hardness, frictional coefficient, and specific wear rate percentages of 94.46, 96.36, and 98.64 were 98.64.
2. based on the findings of an ANOVA. Impacts of the deposition temp and duration on the hardness, frictional coefficient, and wear rate during heating treatment of the electroless coating at a constant CNT amount (0, 35, and 0.7%). The wear rate and frictional coefficient decrease, the hardness increases with increasing deposition duration, and the temp increases from 350 to 400 °C. By increasing the deposition temp from 400 to 450 °C, the hardness, frictional coefficient, and rate of wear decrease.

The temperature (398.13 °C), duration (4 hours), and CNT amount (0.35%) were used for RSM optimization of the contribution process parameters

(amount of CNTs, deposition temp and duration), and the reaction rate (Rate of) was used to determine the hardness, frictional coefficient, and rate of wear for heating treatment of the coating, with a desirable magnitude of 0.99.

6 REFERENCES

Agrawal, R., & Mukhopadhyay, A. (2023). Inclusion of W in electroless Ni–B coating developed from a stabilizer free bath and investigation of its tribological behaviour. *Journal of the Indian Chemical Society*, *100*(4), 100966. https://doi.org/10.1016/j.jics.2023.100966

AL-ABBOODI, T., Yaser, A., & Al-Khafaji;, Z. (2024). REDUCING VIBRATION AND NOISE IN THE OIL SECTOR USING NANOPARTICLE-REINFORCED POLYMERS. *Academic Journal of Manufacturing Engineering*, *2024*(3).

Al-Dulaimi, K. Y., Hammood, S. A., Kadhim, R. H., & Al-Khafaji, Z. (2024). ROLE OF WIRE ELECTRICAL DISCHARGE MACHINING IN THE PROCESS OF MEASURING THE RESIDUAL STRESSES OF WELDS: A REVIEW. *Academic Journal of Manufacturing Engineering*, *22*(3).

Alaa Mohammed Hussein Wai et al. Alaa Mohammed Hussein Wai et al.,. (2019). Comparing the Effect of Heat Treatment and Plasma-Nitriding on Corrosion Resistance of Ni-B-CNT Electroless Coating with Different CNT Concentration on AISI 4340 Steel. *International Journal of Mechanical and Production Engineering Research and Development*, *9*(5), 183–196. https://doi.org/10.24247/ijmperdoct201917

Barman, M., Barman, T. K., & Sahoo, P. (2019). Effect of borohydride concentration on tribological and mechanical behavior of electroless Ni-B coatings. *Materials Research Express*, *6*(12), 126575. https://doi.org/10.1088/2053-1591/ab58b7

Bezerra, M. A., Santelli, R. E., Oliveira, E. P., Villar, L. S., & Escaleira, L. A. (2008). Response surface methodology (RSM) as a tool for optimization in analytical chemistry. *Talanta*, *76*(5), 965–977. https://doi.org/10.1016/j.talanta.2008.05.019

Biswas, P., Das, S. K., & Sahoo, P. (2022). Duplex electroless Ni-P/Ni-Cu-P coatings: Preparation, evaluation of microhardness, friction, wear, and corrosion performance. *Journal of Electrochemical Science and Engineering*. https://doi.org/10.5599/jese.1392

Boccaccini, A. R., & Zhitomirsky, I. (2005). Application of Electrophoretic and Electrolytic Deposition Techniques in Ceramics Processing. Part 1. *ChemInform*, *36*(46). https://doi.org/10.1002/chin.200546219

Bonin, L., Vitry, V., & Delaunois, F. (2020). Replacement of Lead stabilizer in electroless Nickel-Boron baths: Synthesis and characterization of coatings from bismuth stabilized bath. *Sustainable Materials and Technologies*, *23*, e00130. https://doi.org/10.1016/j.susmat.2019.e00130

Bülbül, F., Altun, H., Küçük, Ö., & Ezirmik, V. (2012). Tribological and corrosion behaviour of electroless Ni-B coating possessing a blackberry like structure. *Metals and Materials International*, *18*(4), 631–637. https://doi.org/10.1007/s12540-012-4011-1

Conshohocken, W. (2017). ASTM G99-17, standard test method for wear testing with a pin-on-disk apparatus, ASTM International. *Wear*, *1*, 1–5.

Dawood, N. M., Radhi, N. S., & Al-khafaji, Z. S. (2020). *Investigation Corrosion and Wear Behavior of Nickel-Nano Silicon Carbide on Stainless Steel 316L*. *1002*, 33–43. https://doi.org/10.4028/www.scientific.net/MSF.1002.33

Ghafari, E., Costa, H., & Júlio, E. (2014). RSM-based model to predict the performance of self-compacting UHPC reinforced with hybrid steel micro-fibers. *Construction and Building Materials*, *66*, 375–383. https://doi.org/10.1016/j.conbuildmat.2014.05.064

Haleem, A. H., Radhi, N. S., Jaber, N. T., & Al-Khafaji, Z. (2024). Preparation and Exploration of Nano-Multi-Layers on 316l Stainless Steel for Surgical Tools. *Jordan Journal of Mechanical and Industrial Engineering (JJMIE)*, *18*(2), 339–350.

He, Y., Wang, S. C., Walsh, F. C., Chiu, Y.-L., & Reed, P. A. S. (2016). Self-lubricating Ni-P-MoS2 composite coatings. *Surface and Coatings Technology*, *307*, 926–934. https://doi.org/10.1016/j.surfcoat.2016.09.078

Jabor, M., Radh, N. S., Al-Kinani, M. A., & Al-Khafaji, Z. S. (n.d.). *Optimization of Electro less of Nickel base coating for Cermet Cutting Tools Substrate*.

Jasim Ahmed Jasim;, Yaser, A., & Al-Khafaji, Z. (2024). AN ANSYS SIMULATION STUDY ON THE EFFECT OF APPLYING TITA-NIUM ALLOY (TI-6AL-4V) COATING FOR WIND TURBINE GEAR. *Academic Journal of Manufacturing Engineering*, *22*(4).

Marciano, F. R., Almeida, E. C., Lima-Oliveira, D. A., Corat, E. J., & Trava-Airoldi, V. J. (2010). Crystalline diamond particles into diamond-like carbon films: The influence of the particle sizes on

the electrochemical corrosion resistance. *Surface and Coatings Technology*, *204*(16–17), 2600–2604. https://doi.org/10.1016/j.surfcoat.2010.02.014

Mohammed, E., & Al-khafaji, Z. (2023). Effect of Surface Treatments by Ultrasonic on NiTi Biomaterials. *ACADEMIC JOURNAL OF MANUFACTURING ENGINEERING*, *21*(3), 1–6.

Mukhopadhyay, A., Barman, T. K., Sahoo, P., & Davim, J. P. (2018). Comparative study of tribological behavior of electroless Ni–B, Ni–B–Mo, and Ni–B–W coatings at room and high temperatures. *Lubricants*, *6*(3), 67.

Nabhan, F., Fayyad, E. M., Sliem, M. H., Shurrab, F. M., Eid, K., Nasrallah, G., & Abdullah, A. M. (2023). ZnO-Doped gC(3)N(4) Nanocapsules for Enhancing the Performance of Electroless NiP Coating-Mechanical, Corrosion Protection, and Antibacterial Properties. *ACS Omega*, *8*(25), 22361–22381. https://doi.org/10.1021/acsomega.2c07288

RADHI, N. S., AL-KHAFAJI, Z., MAREAI, B. M., RADHI, S., & ALSAEGH, A. M. (2023). REDUCING OIL PIPES CORROSION BY (ZN-NI) ALLOY COATING ON LOW CARBON STEEL SUBSTRATE BY SUSTAINABLE PROCESS. *Journal of Engineering Science and Technology*, *18*(3), 1624–1638.

Radhi, N. S., Salman, A. J., & Al-Khafaji, Z. (2024). Investigation of in vitro behavior of composite coating hydroxyapatite-nano silver on 316L stainless steel substrate by electrophoretic technic for biomedical tools. *Open Engineering*, *14*(1), 20240017.

Sattar, S., Alaiwi, Y., Radhi, N. S., & Al-khafaji, Z. (2023). Numerical Simulation for Effect of Composite Coating (TiO2 + SiO2) Thickness on Steam Turbine Blades Thermal and Stress Distribution. *ACADEMIC JOURNAL OF MANUFACTURING ENGINEERING*, *21*(4).

Shaikh, S., Sadeghi, M., Cruz, S., & Ferreira, F. (2024). Recent Progress on the Tribology of Pure/Doped Diamond-like Carbon Coatings and Ionic Liquids. *Coatings*, *14*(1), 71. https://doi.org/10.3390/coatings14010071

Tsai, P.-C., Jeng, Y.-R., Lee, J.-T., Stachiv, I., & Sittner, P. (2017). Effects of carbon nanotube reinforcement and grain size refinement mechanical properties and wear behaviors of carbon nanotube/copper composites. *Diamond and Related Materials*, *74*, 197–204. https://doi.org/10.1016/j.diamond.2017.03.012

Vitry, V., Hastir, J., Mégret, A., Yazdani, S., Yunacti, M., & Bonin, L. (2022). Recent advances in electroless nickel-boron coatings. *Surface and Coatings Technology*, *429*, 127937. https://doi.org/10.1016/j.surfcoat.2021.127937

Vitry, V., Sens, A., Kanta, A.-F., & Delaunois, F. (2012). Experimental study on the formation and growth of electroless nickel–boron coatings from borohydride-reduced bath on mild steel. *Applied Surface Science*, *263*, 640–647. https://doi.org/10.1016/j.apsusc.2012.09.126

Wan, Y., Yu, Y., Cao, L., Zhang, M., Gao, J., & Qi, C. (2016). Corrosion and tribological performance of PTFE-coated electroless nickel boron coatings. *Surface and Coatings Technology*, *307*, 316–323. https://doi.org/10.1016/j.surfcoat.2016.09.001

Wang, Q., Callisti, M., Miranda, A., McKay, B., Deligkiozi, I., Milickovic, T. K., Zoikis-Karathanasis, A., Hrissagis, K., Magagnin, L., & Polcar, T. (2016). Evolution of structural, mechanical and tribological properties of Ni–P/MWCNT coatings as a function of annealing temperature. *Surface and Coatings Technology*, *302*, 195–201. https://doi.org/10.1016/j.surfcoat.2016.06.011

7 NOTATION

The following symbols are used in this paper:
A_{cc} = area of core concrete;
A_t = total area